

3D MEMS Simulation Modeling Using Modified Nodal Analysis

J. V. Clark, N. Zhou, D. Bindel,
L. Schenato, W. Wu,
J. Demmel, K. S. J. Pister

Berkeley Sensor and Actuator Center
497 Cory Hall, University of California at Berkeley
Berkeley CA, USA, cfm@bsac.eecs.berkeley.edu

ABSTRACT

The modeling, simulation, and experimental verification of several MEMS devices are presented. Simulated results include 3D mode analysis, residual stress effects, thermal expansion, nonlinear deflections, time-varying electrostatic forces, process sensitivities, induced currents, and the transient performance in accelerated reference frames. To simulate the performance of these MEMS devices a modified nodal analysis approach is used to formulate a system of ODEs that is solved by static, steady state, and transient solvers.

Index Terms - SUGAR, modified nodal analysis, static, steady state, transient, accelerating frames, sensitivity.

1 INTRODUCTION

SUGARv1.1 is a collection of MATLAB [1] algorithms that take a netlist description of MEMS devices and perform static, steady-state, model, and transient analyses of three-dimensional mechanical structures and electrical circuits. The code, demo files, and manual are downloadable from the Berkeley Sensor and Actuator Center at the University of California at Berkeley [2]. NODAS [3] performs similar MEMS nodal analysis.

SUGAR uses a SPICE-like [4] environment where a netlist provides the geometry and connectivity of each component, a process file provides the process parameters (e.g. Young's modulus, Poisson's ratio, coefficient of thermal expansion, residual stress, etc), and new component models can be easily added. Creating a netlist and obtaining speedy results is a simple process in SUGAR. For example, the following netlist and commands display the second mode of a cantilever beam.

```
%Modelname Layer [nodes] [parameters]
anchor p1 [a X][l=5u w=10u oz=180 h=4u]
beam p1 [a b][l=100u w=2u y=0 oz=0 ox=0]
```

```
%Matlab commands:
[net] = cho_load('cantilever.net'); %load netlist
[f, egv, dq] = cho_mode(net); %mode calculation
mode = 2; scale = 0.7;
cho_modeshape(net, egv, dq, scale, mode); %3D display
```

Sections two and three below describe the models and algorithms used in the simulations, which are presented in section four.

2 MODELING

2.1 MEMS Representation in SUGAR

Many microelectromechanical systems can be represented by lumped models and their performance can be described by parameterized ODEs

$$M\ddot{q} + D\dot{q} + Kq = \Sigma F \quad (1)$$

where coefficients M , D , and K represent the mass, damping, and stiffness system matrices. The three-dimensional displacement and excitation vectors for a system of N nodes ($6N$ degrees of freedom) are

$$q_i = \begin{bmatrix} q_{xi} \\ q_{yi} \\ q_{zi} \\ q_{\theta xi} \\ q_{\theta yi} \\ q_{\theta zi} \end{bmatrix}, F_i = \begin{bmatrix} F_{xi} \\ F_{yi} \\ F_{zi} \\ M_{xi} \\ M_{yi} \\ M_{zi} \end{bmatrix}, q = \begin{bmatrix} q_1 \\ q_2 \\ q_3 \\ q_4 \\ \vdots \\ q_N \end{bmatrix}, F = \begin{bmatrix} F_1 \\ F_2 \\ F_3 \\ F_4 \\ \vdots \\ F_N \end{bmatrix}, \quad (2)$$

The q_i 's consist of displacement translations and rotations about global axes. The F_i 's are the corresponding forces and moments. Any electrical elements are appended onto these elements, creating vectors of length $6N_{Mechanical} + N_{Electrical}$.

The parameterized M_i , K_i , and D_i elements for a linear beam model can be shown to be [5]

$$T_i = \begin{bmatrix} \Psi_i & & & \\ & \Psi_i & & \\ & & \Psi_i & \\ & & & \Psi_i \end{bmatrix} \quad (7)$$

where Ψ_i is the direction cosine matrix corresponding to the orientation of element i .

Nonlinear beam elements are currently supported in two dimensions.

2.2 Thermal Expansion

The current thermal model assumes a constant temperature along each beam. The temperature of a beam is specified in the netlist. The ambient temperature is specified in the process file.

Using equation (1), the linear displacement of a MEMS device due to thermal expansion is given by

$$\begin{aligned} q &= K^{-1} F_{Thermal} \\ F_{Thermal} &= A \sigma \\ \sigma &= E \alpha \Delta T \end{aligned} \quad (8)$$

where

$$\begin{aligned} E &= \text{Young's modulus} \\ \Delta T &= T_{beam} - T_{ambient} \\ \alpha &= \text{coefficient of thermal expansion} \\ \sigma &= \text{thermal stress} \\ A &= \text{cross sectional area} \end{aligned}$$

2.3 Residual Stress

The method used for the determination of static equilibrium due to stress and strain gradients is similar to the above analysis. Given a residual stress, the static deflection is

$$\begin{aligned} q &= -K^{-1} F_{Stress} \\ F_{Stress} &= A \sigma \end{aligned} \quad (9)$$

where

$$\begin{aligned} \sigma &> 0, \text{ tensile (beam shortening)} \\ \sigma &< 0, \text{ compressive (beam lengthening)} \end{aligned}$$

Likewise, for the strain gradient Γ specified in the process file, the deflection is obtained by the moments acting on each node

$$\begin{aligned} q &= K^{-1} M_{Strain} \\ M_{Strain} &= EI_y \Gamma \end{aligned} \quad (10)$$

where

$$\begin{aligned} M &= \text{moment} \\ \Gamma &> 0, \text{ concave up} \\ \Gamma &< 0, \text{ concave down} \end{aligned}$$

2.4 Accelerating Frames

For non-inertial reference frames, i.e. accelerating and rotating substrates, SUGAR solves the following ODE

$$M\ddot{q} + D\dot{q} + Kq = F_{Electrostatic}(t, q) + F_{Inertial}(t) \quad (11)$$

where $F_{Electrostatic}$ are forces due to the on-chip electrostatic actuators (see section 2.5), and $F_{Inertial}$ are the inertial forces due to the accelerating frame given by

$$F_{Inertial} = M\ddot{R} - M\omega \times (\omega \times r) - 2M\omega \times \dot{r} - M\dot{\omega} \times r \quad (12)$$

$$\begin{aligned} \text{where } M &= 3D \text{ system mass matrix} \\ R(t) &= \text{substrate position vector} \\ \omega(t) &= \text{angular frequency vector} \\ r(t) &= \text{node position vector} \end{aligned}$$

and where the terms on the right side of equation (12) correspond to the translational, centrifugal, Coriolis, and transverse forces respectively.

2.5 Electrostatic Gap

Since SUGAR is node based, the distributed forces along the beam of an electrostatic gap must be formed into equivalent node forces and moments. This is accomplished by integrating the electrostatic load $p(x)$ multiplied by the Hermitian shape function $H(x)$ along the length of the beams [5]

$$\begin{aligned} F_{Electrostatic,i} &= \int_0^L p(x) H_i(x) dx \\ p(x) &= \frac{-1}{2} \frac{\epsilon_o h V^2 \alpha(d(x))}{d(x)^2} \end{aligned} \quad (13)$$

where

$$\begin{aligned} H_i(x) &= \text{Hermitian shape functions} \\ p(x) &= \text{electrostatic load} \\ V &= \text{voltage} \\ d(x) &= \text{gap distance} \\ \epsilon_o &= \text{permittivity of free space} \\ h &= \text{layer thickness} \\ \alpha(x) &= \text{fringing field factor} \end{aligned}$$

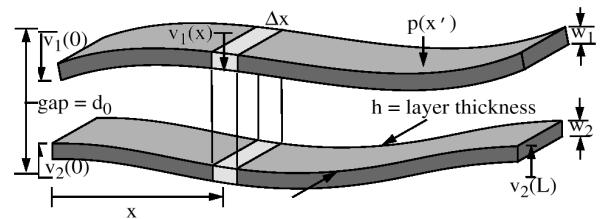


Figure 1: Gap model parameters defined.

3 ALGORITHMS

3.1 Static Analysis

SUGAR uses a modified Newton-Raphson algorithm to find an equilibrium state when one or more nonlinear elements or excitations are entered in the netlist. The determination of multiple equilibria (e.g. buckling) is not implemented. Given a system subject to nonlinear excitations of various energy domains (e.g. thermal, electrical, mechanical), the system is in static equilibrium when

$$f(q) = 0 \quad (14)$$

where the function f contains the modified nodal equation for each energy domain that represents the particular system. For a system containing mechanical and electrical elements, equation (14) represents a state where all nodal forces, moments, and electric currents sum to zero.

SUGAR solves equation (14) using Newton's method with stopping criterion

$$\|q_{n+1} - q_n\| < \zeta \quad (15)$$

where ζ is the selected tolerance.

3.2 Steady-State Analysis

To determine the steady-state response, SUGAR first linearizes the system of ordinary differential equation at the point of static equilibrium. The high order system of ODEs is then converted into first order form given by

$$\begin{aligned} \dot{x} &= Ax + Bu \\ y &= Cx + Du \end{aligned} \quad (16)$$

where x is the system dynamic state variable, u is the sinusoidal excitation, and y is the system dynamic response. A , B , C , and D are the system, input coupling, output, and feed forward matrices respectively [6]. The solution of equation (16) provides Bode plots as well as modal analysis.

3.3 Transient Analysis

This solver calculates the transient response of a MEMS device, which may contain nonlinear elements and excitations that are functions of time t and state vector q . Several ODE solvers are available, whereby speed may be traded for accuracy and long-term stability. These

numerical methods include an implicit second order Rosenbrock solver for stiff problems where low accuracy is acceptable, an explicit Runge-Kutta 4th-5th order solver for non-stiff systems, an implicit multi-step integration method of varying order for stiff problems requiring higher accuracy, and a simple explicit Euler algorithm. The transient solvers require the system ODEs to be in first order form. We do this in the standardized way [7] by introducing a new state vector Q where

$$\dot{Q} \equiv \frac{d}{dt} \begin{bmatrix} q \\ \dot{q} \end{bmatrix} = f(t, q) \quad (17)$$

3.4 Sensitivity Analysis

The predicted performance of MEMS is subject to process variations that occur during the fabrication stage. Small variations in geometry may lead to performance which is substantially different from the ideal. SUGAR models this effect by perturbing the system stiffness matrix K .

For static analysis

$$F = [K(g) + \Delta K(\delta)]q \quad (18)$$

where g contains the ideal layout geometry and process file parameters. δ is the variation in g given by Gaussian, uniform, or uniform distribution of corners. The perturbation in stiffness, $\Delta K(\delta)$, is determined by both probabilistic and deterministic techniques.

A Monte-Carlo algorithm [8] evaluates the most likely outcome of equation (18) by drawing many samples from a random distribution of geometric variables.

Given the bounds on the geometric variables, an Ellipsoidal Calculus technique [9] is used to find the extreme bounds on performance parameters, i.e. the worst-case scenario.

4 RESULTS

4.1 Residual Stress Effects

MEMS are often subject to residual stresses that depend on the fabrication technique. Residual stress may affect device geometry and performance. Figure 3 shows a simulation of compressive stress applied to a residual stress gauge designed by C. Pan and W. Hsu. Simulated deflection is within 0.59% of measured data [10].

Some fabrication methods produce material layers with stress that is a function of layer depth. Figure 4 shows the static deflection of a simplified XL-05 accelerometer. The strain gradient term in this simulation is magnified to highlight the doming up of the backbone and the bending down of the comb-drive electrodes. The actual negative strain gradient for this particular process is such that a 150 μm cantilever beam will typically deflect down 0.3 μm , which is in good agreement with SUGAR [11].

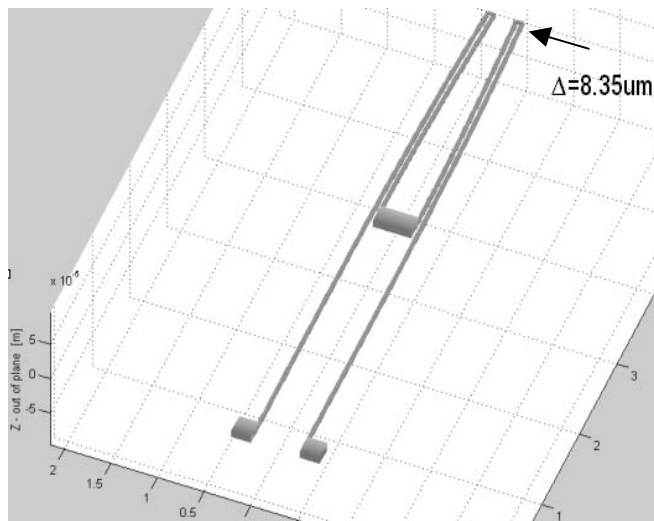


Figure 3: Residual stress gauge

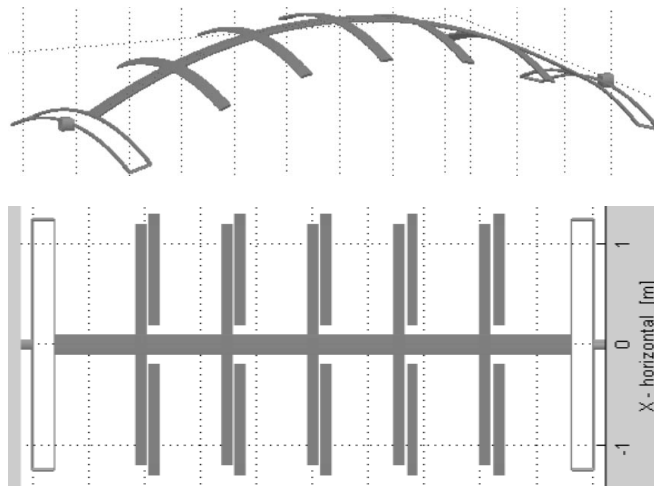


Figure 4 Strain gradient example.

4.2 Thermal Expansion

SUGAR uses a limited thermal model where each beam may be assigned a constant temperature. In the real device temperature is distributed along the length of the beam [12], where temperature is a function of electric current through the beam, atmospheric convection, conduction from

attached elements, and sources of radiation. By applying an average temperature to each beam element in a heatuator design, SUGAR comes within 6% of the measured tip deflection provided by P. Allen et. al. [13]. Figure 5 shows, the average temperatures of the hot arm, cold arm, and tip displacement.

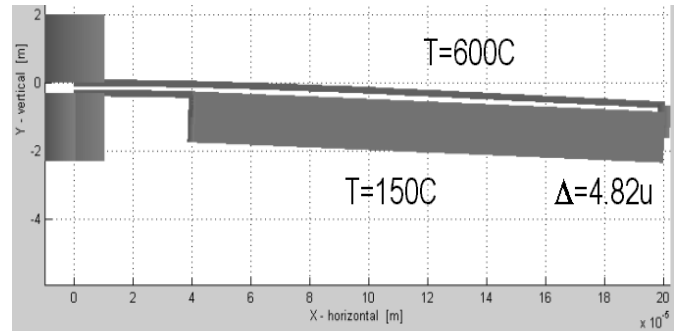


Figure 5: Thermal deflection of a heatuator.

4.3 Nonlinear Stiffness

Figure 6 shows the simulation of a 4-bit MEM-DAC (microelectromechanical digital to analog converter) designed by R. Yeh, B. Murmann, and K. Pister [14]. Figure 6a plots simulation against measured data. The linear beam model fits the ideal converter case; however, measured data reveals nonlinearities in the device performance. This can be attributed to large beam deflections. SUGAR's nonlinear beam model more accurately predicts experimental data, where stiffness is a function of displacement.

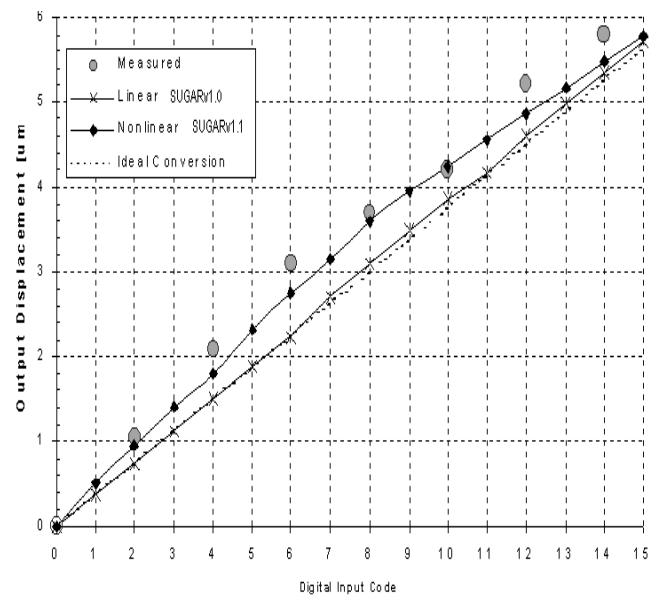


Figure 6a: MEM-DAC data.

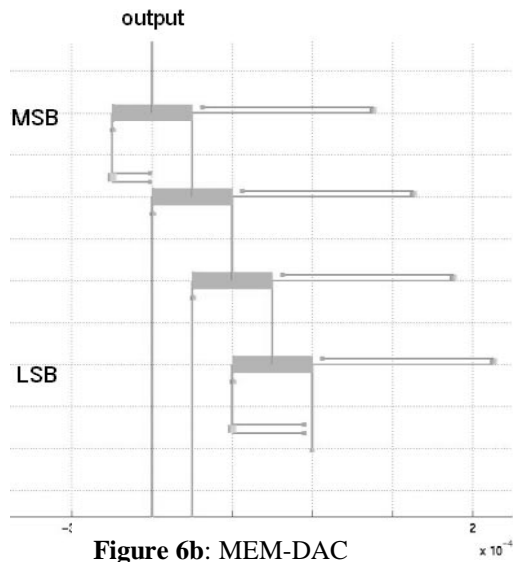


Figure 6b: MEM-DAC

4.4 Transient Response

Figure 7b shows the transient response to the gap-closing actuator in 7a. An initial voltage is applied across the gap, which increases linearly in time. Displacement of node C is shown as a function of time. The initial voltage step starts the device to resonate. As the voltage increases at a linear rate, the gap decreases at a nonlinear rate due to the electrostatic force increasing as $\sim 1/gap^2$. This force also causes the period of oscillation to increase. Once the voltage is removed, the actuator exponentially decays back to equilibrium due to viscous air damping.

Figure 8 shows the response of a simple gyro subject to a spinning substrate. The gyro is first set in motion along the y-axis. The plots show the E_y and E_x displacements of node E as functions of time. Midway through the simulation the left anchor is set to spin about the z-axis at 1 rad/sec. Though this angular velocity has almost no effect on E_y , E_x is significantly affected.

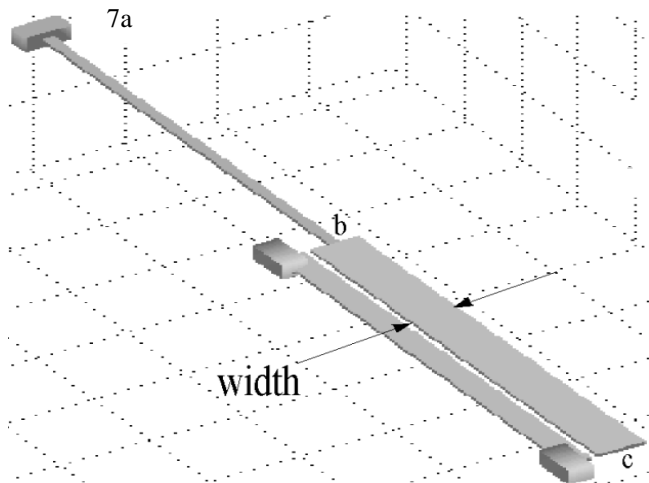


Figure 7a: Gap-closing actuator.

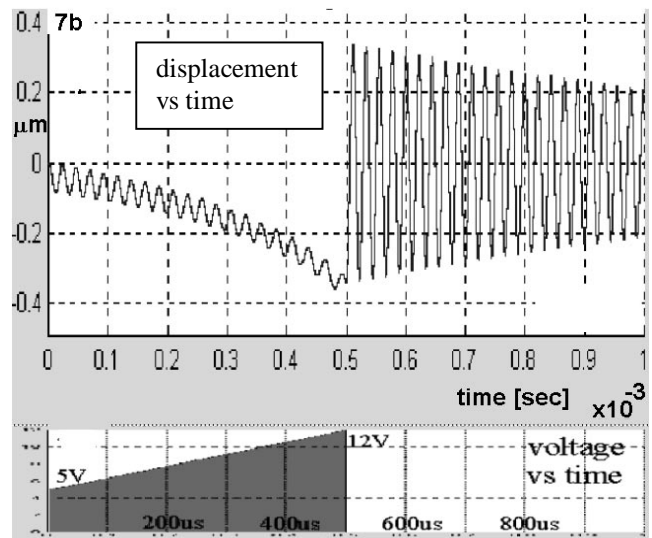


Figure 7b: Dynamics of a gap-closing actuator.

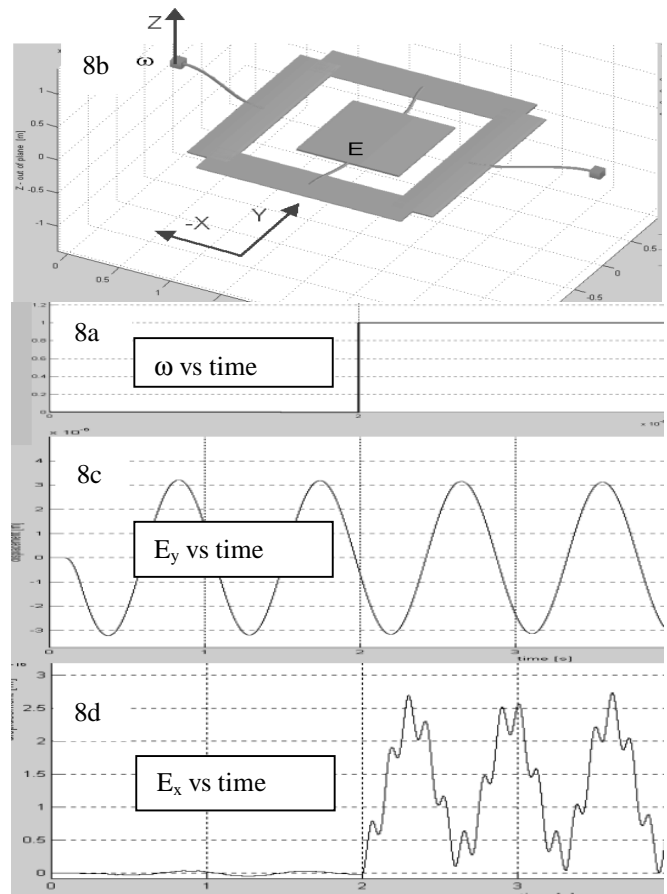


Figure 8: Gyro in accelerating frame.

4.5 Process Variation Analysis

In this simulation a $100\mu\text{N}$ vertical force is applied at the lower-middle node of the dog-bone suspension shown in figure 9. Ideally, a symmetric structure such as this

would only generate vertical displacement. However, due to variations in geometric variables, the node also experiences rotational displacement. Figure 9b shows possible displacements due to a uniform distribution of geometric variables and worst-case ellipsoid. The results from a uniform corner distribution is shown in figure 9c, where it is more likely that solutions could fall on the ellipsoid boundary of 100% confidence.

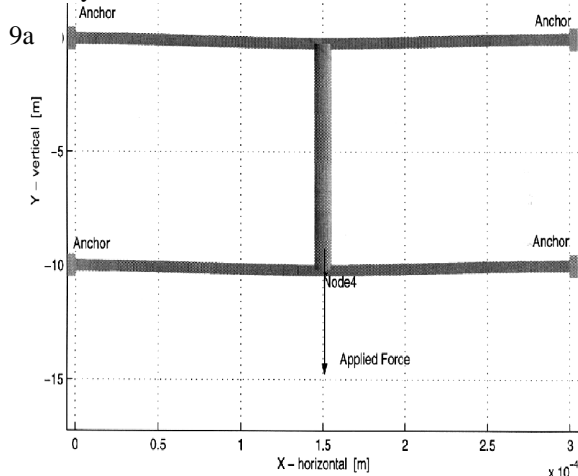


Figure 9a: Geometrical variation analysis.

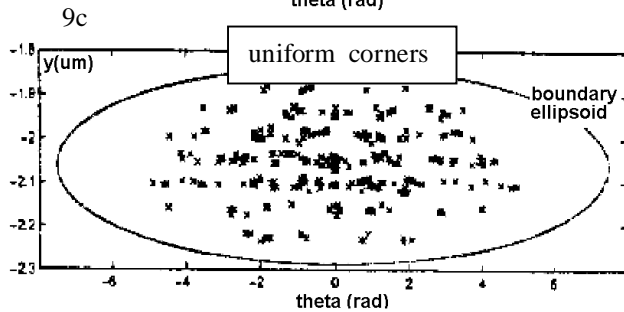
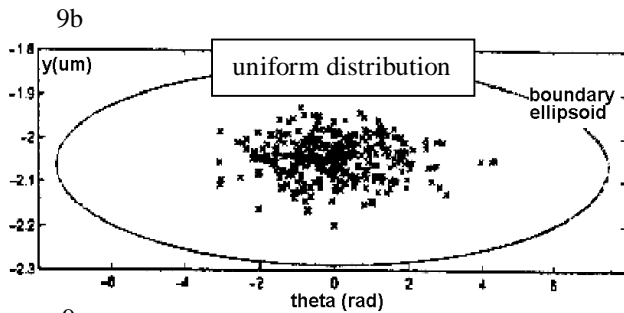


Figure 9b-c: Geometrical variation analysis.

4.6 Steady-State Response

Figure 10 shows steady-state analysis performed on a multi-domain system, where electrostatic forces are applied to coupled mechanical and electrical elements.

Figure 10a shows a simulation of the induced current produced by a multi-mode resonator designed by R. Brennan [15]. Figure 10b shows the Bode and phase plot for the induced current of the sensing comb as a function of

frequency of the voltage at the driving comb. The measured modes are within 5% of experimental frequencies.

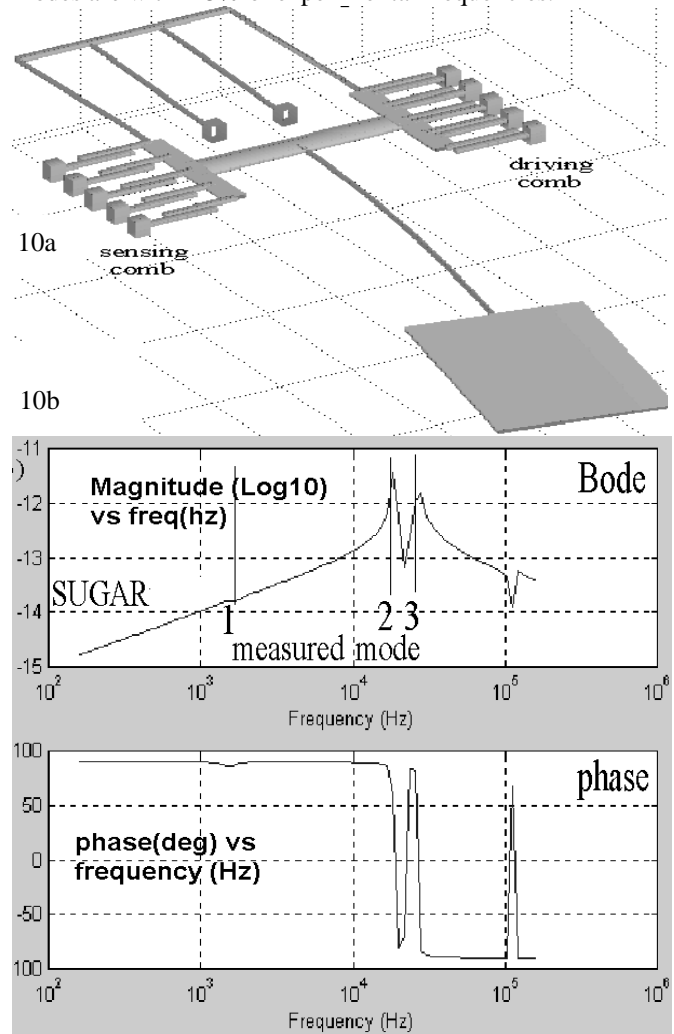


Figure 10: Steady-state response of induced current.

4.7 3D Modal Analysis

The final example demonstrates the use of three-dimensional modal analysis performed on a gyro prototype designed by A. Seshia and R. T. Howe [16].

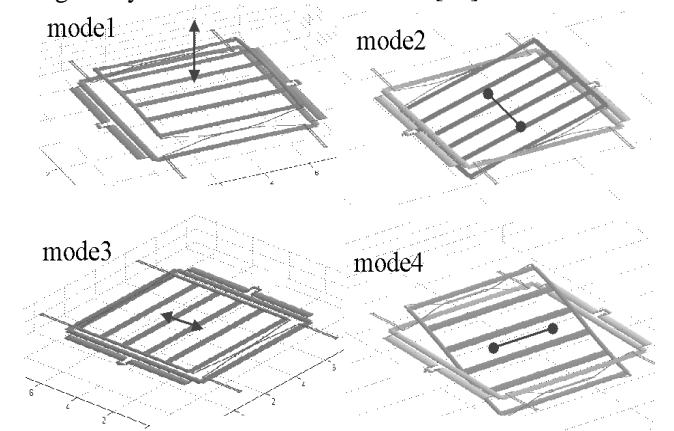


Figure 11: First 4 mode shapes.

5 CONCLUSIONS

We have shown that a MEMS modified nodal analysis environment modeled on SPICE can predict the performance of a variety of MEMS devices. SUGAR currently incorporates static, steady-state, modal, transient, and sensitivity solvers. Further development may include bifurcation phenomena, model reduction, contact problems, efficient modeling of multi-scale physics, and industry standard CIF file readability. SUGAR is also being made available through U. C. Berkeley's Millennium web service [17] to internal Berkeley users, and eventually to external users.

ACKNOWLEDGMENT

The authors would like to thank R. T. Howe, A. Seshia, and R. Connant for helpful discussions.

REFERENCES

- [1] MATLAB, High-Performance Numeric Computation and Visualization Software, *The Math Works Inc.*, 24 Prime Park Way Natick, Mass.
- [2] <http://www-bsac.eecs.Berkeley.edu/~cfm>
- [3] J. Vandemeer, "Nodal Design of Actuators and Sensors (NODAS)," M.S. Thesis
- [4] L. W. Nagel, "SPICE2: A Computer Program to Simulate Semiconductor Circuits," *ERL Memo. No. UCB/ERL Vol M75/520* (1975)
- [5] J. V. Clark, N. Zhou, K. S. J. Pister, "MEMS Simulation Using SUGARv0.5," *Tech. Digest, Solid-State Sensor and Actuator Workshop*, Hilton Head Island SC, pp.191-196, Jun8-11 (1998).
- [6] Norman S.Nise, "Control System engineering," *The Benjamin/Cummings Publishing, Inc,CA* (1991)
- [7] S. Sastry, "Nonlinear Systems Analysis, Stability, and Control," *Springer* (1999)
- [8] D.J.C MacKay, "Introduction to Monte Carlo Methods," *M. I. Jordan*, (1999)
- [9] G. Calafiore, L. El Ghaoui, "Confidence ellipsoids for uncertain linear equations with structure," *In Proceedings of the IEEE CDC*, (1999)
- [10] Chi. Pan, W. Hsu, "A Microstructure for In Situ Determination of Residual Strain," *Journal of Microelectromechanical Systems*, vol 8, No. 2, June (1999)
- [11] Personal communication with R. T. Howe.
- [12] Conant, R.A., R. S. Muller, "Cyclic Fatigue Testing of Surface-Micromachined Thermal Actuators," *presented at the 1998 ASME Internation Mechanical Engineering Congress and Exposition*, Nov 15-20, 11998, Anaheim, CA, DSC-Vol. 66, pp. 273-277.
- [13] P. Allen, J. Howard, E. Kolesar, J. Wilken, "Design, Finite Element Analysis, and Experimental Performance Evaluation of a Thermally-Actuated Beam Used to Achieve Large In-Plane Mechanical Deflections," *Tech. Digest, Solid-State Sensor and Actuator Workshop*, Hilton Head Island SC, pp.191-196, Jun8-11 (1998).
- [14] Yeh, R., Conant, R., and Pister, K.S.J., "Mechanical Digital to Analog Converter," *Proc. The Tenth International Conference on Sensors and Actuators (Transducers '99)*, Sendai, Japan, June 7-10, 1999, pp. 998-1001.
- [15] R. Brennen, A. Pisano, W. Tang, "Multiple Mode Micromechanical Resonators," *Proc. IEEE Micro Electro Mechanical Systems Workshop* (1990).
- [16] Personal communication with A. Seshia.
- [17] <http://www.millennium.berkeley.edu>